



International Conference on the Technology of Plasticity, ICTP 2017, 17-22 September 2017,  
Cambridge, United Kingdom

## Hot deformation behavior of n-ODS-18Cr steel

J. Rajesh<sup>a,\*</sup>, R. Vijay<sup>b</sup>, S. Ganesh Sundara Raman<sup>a</sup> and G. Sundararajan<sup>a</sup>

<sup>a</sup>Department of Metallurgical and Materials Engineering, Indian Institute of Technology Madras, Chennai-600036, India

<sup>b</sup>Centre for Nanomaterials, International Advanced Research Centre for Powder Metallurgy and New Materials, Hyderabad-500005, India

### Abstract

In the present work, nano oxide dispersion strengthened (ODS) steel was prepared by high energy ball milling of the elemental powders, followed by canning and upset forging. The chemical composition of the material used in this study is Fe-17.8Cr-2.33W-0.23Ti-0.35Y<sub>2</sub>O<sub>3</sub>. Isothermal compression tests were carried out on upset forged ODS-18Cr steel samples over a range of temperatures (1273 to 1423 K) and strain rates (10<sup>-2</sup> s<sup>-1</sup> to 10 s<sup>-1</sup>) utilizing Gleeble-3800 machine. Transmission electron microscopy and electron back scattered diffraction were carried out on the deformed samples to evaluate the grain size and to identify dynamic recrystallized grains. The true stress- true strain data obtained from compression tests at different strain rates were also utilized to estimate and rationalize the activation energy for deformation and the stress exponent. The obtained deformation mechanism parameters are greater than those for the non-ODS steels, which is attributed to the threshold stress generated due to dislocation/particle interaction. Sellars-Tegart equation was used to predict the peak flow stress and the predicted results were comparable to the experimental results.

© 2017 The Authors. Published by Elsevier Ltd.

Peer-review under responsibility of the scientific committee of the International Conference on the Technology of Plasticity.

*Keywords:* ODS-18Cr steel, Upset forging, Microstructure, Constitutive equation

### 1. Introduction

Nano oxide dispersion strengthened (n-ODS) steels are considered as candidate materials in generation IV fast

\* Corresponding author. Tel.: +91-8801048602; fax: +0-000-000-0000 .  
E-mail address: [rajeshjarugula@gmail.com](mailto:rajeshjarugula@gmail.com)

breeder nuclear reactors due to their superior properties such as high temperature strength, high swelling resistance and high resistance to corrosion and oxidation [1, 2]. Addition of Titanium to these steels to form  $Y_2Ti_2O_7$  and  $Y_2TiO_5$  nano-particles, and controlling the size of these nano-particles are crucial for high temperature strength and resistance to irradiation [3, 4]. This is owing to the matrix-particle interface, which acts as a sink for He bubbles. The nano-particles present in the steel matrix and the processing route (such as high energy ball milling, hiping, upset forging and hot extrusion) of ODS steels influence the microstructure during hot deformation. Therefore, optimization of these parameters to obtain the required microstructure during hot working conditions is important. Most of the literature available on ODS-9Cr, 12Cr and 14Cr steels show that these steels possess less corrosion and oxidation resistance. Advanced nuclear reactors require high corrosion resistance materials to be compatible with sodium and nitric acid. It is well known that corrosion resistance increases with increasing the Chromium content. More attention should be given to the development of ODS-18Cr steels, since they exhibit high corrosion resistance and a single phase at high temperatures [5].

Sellers and Tegart developed a hyperbolic sine Arrhenius-type constitutive equation, which is used to represent the deformation behavior of material in mathematical form [6]. Subsequently, this equation has been modified several times and the revised equation is compensated with strain and strain rate terms. This equation could be used to provide the input data to a finite element code to analyze the material deformation response during simulation under specified loading conditions. However, the reliability of the numerical techniques depends on the accuracy of the constitutive equation obtained from the experimental data. Samantaray et al. studied the hot deformation behavior and proposed a constitutive model for the prediction of flow stress of 9Cr-1Mo steel [7]. Zhang et al. studied the hot deformation and development of processing map of ODS-9Cr steel to optimize the processing conditions [8].

It is found that a limited work has been carried out on the hot deformation behavior of ODS steels. In the present study, hot deformation behavior of ODS-18Cr steel was investigated at a range of temperatures and strain rates. The main aim of the work is to study the microstructural evolution and development of a constitutive equation to predict the flow stress.

### Nomenclature

$\sigma, \sigma_p$	Flow stress and peak flow stress (MPa)
$\dot{\epsilon}$	Strain rate ( $s^{-1}$ )
Q	Activation energy (kJ/mol)
n	Stress exponent
T	Temperature (K)
R	Gas constant (J/mol. K)
$n_1, \beta, \alpha, A$	Material constants

## 2. Experimental Procedure

The ODS-18Cr steel used in this work was synthesized by mechanical alloying of powders followed by upset forging at 1323 K. The chemical composition of the steel studied is given in Table 1. Cylindrical specimens of 10 mm diameter and 15 mm length were cut from the upset forged billet. Isothermal compression tests were carried out in a Gleeble 3800 at a range of temperatures from 1273 to 1423 K with an interval of 50 K and a range of true strain rates from  $0.01 s^{-1}$  to  $10 s^{-1}$ . Specimens were heated at a heating rate of  $5 ^\circ Cs^{-1}$  and held for 300 s at the deformation temperature, and after deformation samples were quenched immediately by water. The specimens were deformed to a true strain of 0.7. For microstructural studies, the samples were cut in the direction parallel to compression axis. Transmission electron microscopy (TEM) was carried out on an FEI-Tecna G2 microscope operated at 200 kV. For TEM examination, thin foils were obtained by mechanical polishing to  $\sim 60 \mu m$  thickness and further thinning was done by twin jet electro polishing using an electrolyte of 90% acetic acid and 10% perchloric acid. Electron back scattered diffraction (EBSD) imaging was carried out using a TSL system on FEI-Inspect F microscope operated at 20 kV and step size used was 50 nm. For EBSD analysis, samples were ground using different SiC sheets and final polishing was done by electro polishing at 20 V.

Table 1 Chemical composition (wt%) of ODS-18Cr steel

Cr	W	Ti	Y <sub>2</sub> O <sub>3</sub>	C	O <sub>total</sub>	O <sub>excess</sub>
17.8	2.33	0.23	0.35	<0.03	0.18	0.1

### 3. Results and Discussion

#### 3.1 Microstructure

The microstructure and grain size distribution of the material are shown in Fig. 1. A bimodal grain structure with very fine grains (recrystallized) of 300 nm size and large grains (un-recrystallized) of 10 μm size was observed. The true stress – true strain curves at 1273 and 1423 K are shown in Fig. 2. Initially the flow stress increased with increasing strain due to initiation of dislocations and their interaction with dislocations and grain boundaries (work hardening) and after stress reached a peak value, flow softening (dislocation annihilation) was observed. The flow stress increased with an increase in strain rate due to increase in dislocation density. More flow softening was observed at 1423 K and particularly at lower strain rates (0.01 and 0.1 s<sup>-1</sup>) compared to that at 1273 K. The temperature dependent mechanisms may be responsible for the decrease in flow stress with increasing temperature.

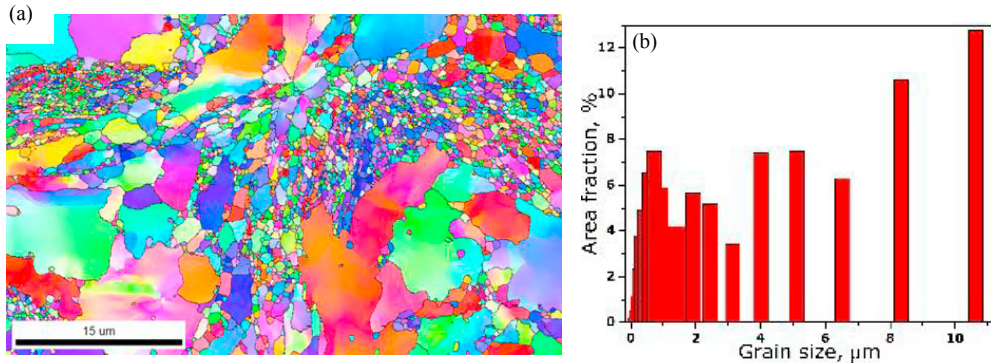


Fig. 1 (a) Microstructure (Inverse pole figure (IPF) image) of as-received material (Upset forged at 1323 K), (b) Grain size distribution

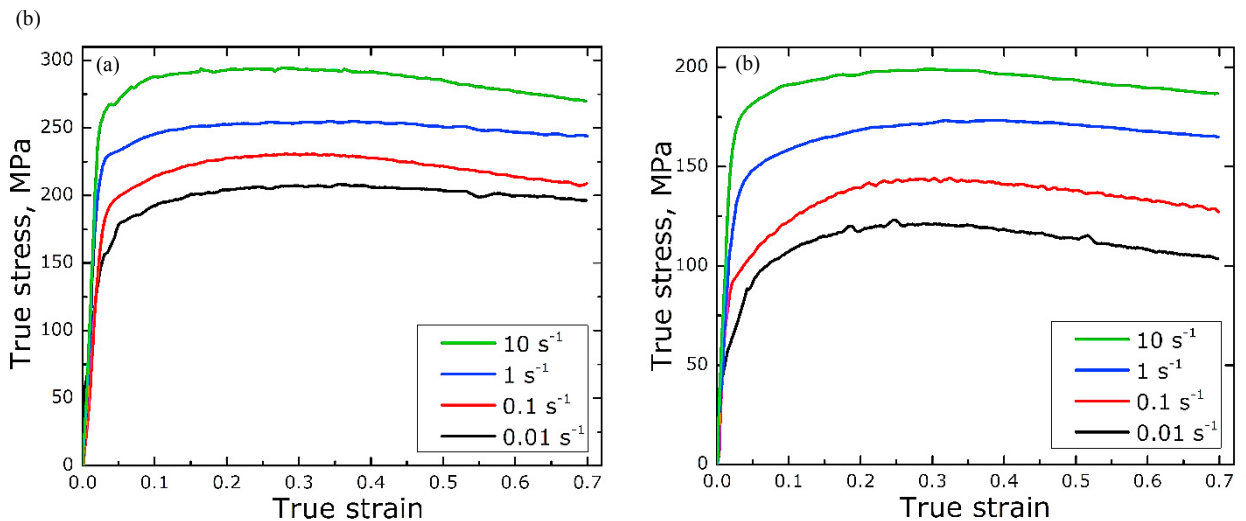


Fig. 2 True stress – true strain curves at different strain rates and two different temperatures: (a) 1273 K, (b) 1423 K

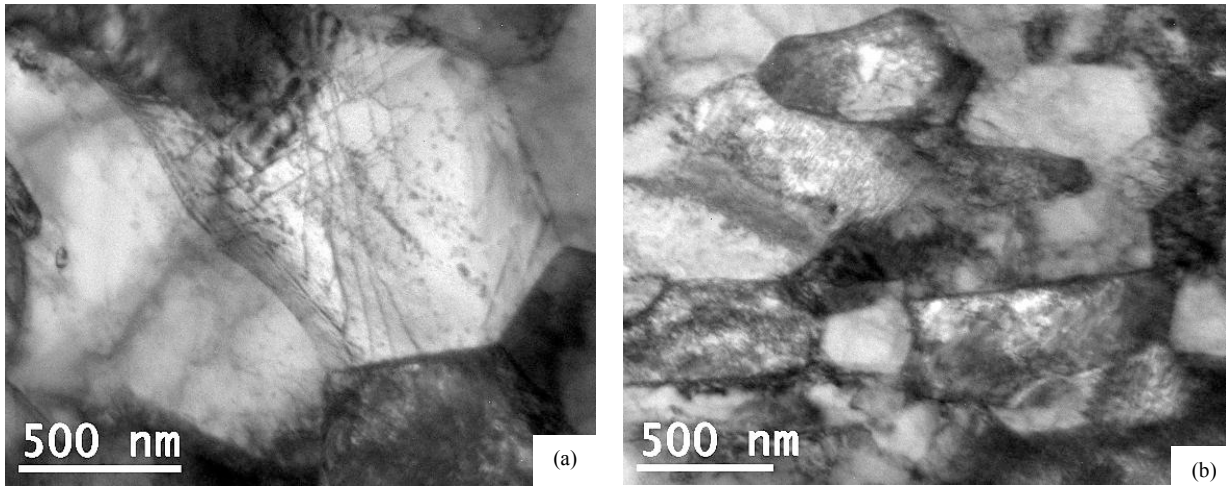


Fig. 3 TEM bright field micrographs of samples deformed at 1423 K and two different strain rates: (a)  $0.01 \text{ s}^{-1}$ , (b)  $10 \text{ s}^{-1}$

TEM micrographs of samples deformed at 1423 K and two different strain rates ( $0.01$  and  $10 \text{ s}^{-1}$ ) are shown in Fig. 3. At both strain rates, grains were elongated normal to the compression direction. The average grain size values are  $0.7 \mu\text{m}$  and  $0.55 \mu\text{m}$  at  $0.01$  and  $10 \text{ s}^{-1}$  respectively. Relatively a high dislocation density was observed in the sample deformed at  $10 \text{ s}^{-1}$ . At a lower strain rate of  $0.01 \text{ s}^{-1}$ , because of higher deformation time, dislocation annihilation is expected to be more. From Fig. 3(a), it is evident that dislocations pinned by particles are distributed within the grain.

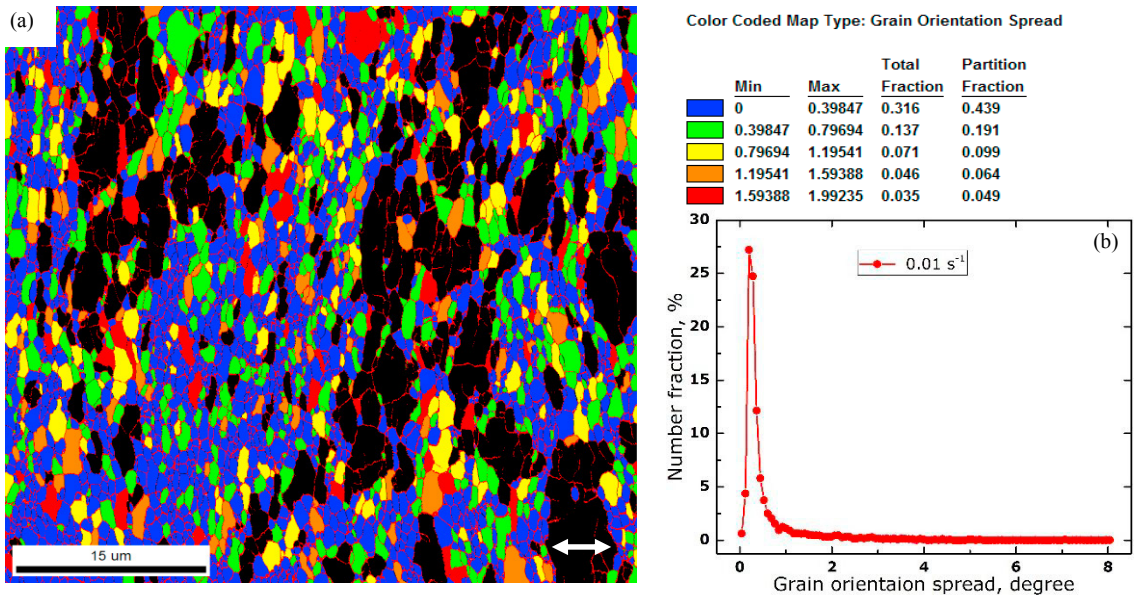


Fig. 4 (a) Microstructure (DRX grains partitioned image) of a deformed sample at 1423 K,  $0.01 \text{ s}^{-1}$  (the arrow indicates the compression direction), (b) GOS distribution of a deformed sample at 1423 K,  $0.01 \text{ s}^{-1}$

From the TEM micrographs, it was difficult to identify whether the material underwent dynamic recrystallization (DRX). In order to identify the DRX grains in the deformed samples, grain orientation spread (GOS) technique was employed. GOS gives the average orientation difference between average grain orientation and all measurements within the grain [9]. GOS distribution can be used to identify recrystallized grains from deformed matrix. In general, lower value of GOS (typically  $< 2^\circ$ ) indicates completely recrystallized grains. From the sample deformed at 1423 K and  $0.01 \text{ s}^{-1}$ , DRX grains were partitioned from the deformed grains as shown in Fig. 4(a) and the GOS distribution is

shown in Fig. 4(b). The peak in the curve with low GOS represents the DRX grains. The area fractions of DRX grains identified in the samples deformed at 0.01 and 10 s<sup>-1</sup> were about 70% and 40% respectively. The values of strain rate sensitivity (m) were determined from Fig. 5(a). Although the peak stress values do not correspond to same strain at different strain rates, this method was used to get an idea of the m value. It may be seen that the obtained m values are not high enough to provide efficient hot working conditions.

### 3.2 Constitutive equation

The effects of temperature and strain rate on deformation behavior could be represented by Zener-Holloman parameter (Z) in an exponent type equation. In the case of hot deformation, the Arrhenius equation is used to describe the relationship between flow stress, strain rate and temperature.

$$Z = \dot{\epsilon} \exp\left(\frac{Q}{RT}\right) \tag{1}$$

$$\dot{\epsilon} = AF(\sigma)\exp\left(-\frac{Q}{RT}\right) \tag{2}$$

$$\begin{aligned} \text{Where, } F(\sigma) &= \sigma^{n_1} & \alpha\sigma < 0.8 \\ F(\sigma) &= \exp(\beta\sigma) & \alpha\sigma > 1.2 \\ F(\sigma) &= [\sinh(\alpha\sigma)]^n & \text{for all } \sigma \end{aligned}$$

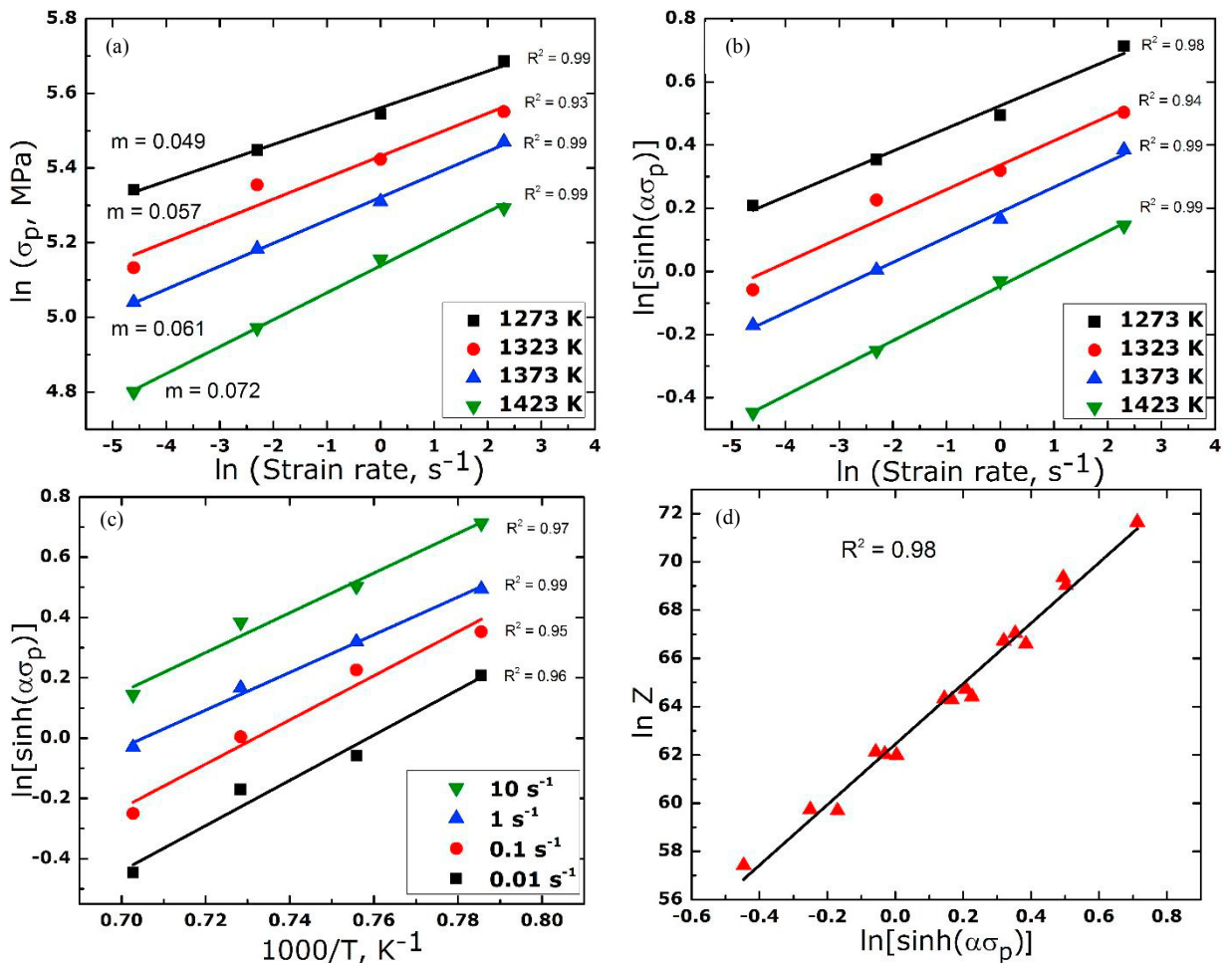


Fig. 5(a) plot of  $\ln \sigma_p$  vs  $\ln$  strain rate, (b) plot of  $\ln [\sinh(\alpha\sigma_p)]$  vs  $\ln$  strain rate, (c) plot of  $\ln [\sinh(\alpha\sigma_p)]$  vs  $1000/T$  and (d) plot of Zener parameter and peak stress

The variation of peak flow stress with strain rate and temperature are shown in Fig. 5. The values of  $\beta$  and  $n_1$  were calculated from the average slopes between  $\sigma_p$  versus  $\ln$  strain rate and  $\ln \sigma_p$  versus  $\ln$  strain rate (Fig. 5(a)). From that the value of  $\alpha$  was calculated as,  $\alpha = \beta/n_1 = 0.00496$ . Deformation mechanism parameters  $n$  (12.53) and  $Q$  (734 kJ/mol) were obtained from the average of slopes between  $\ln [\sinh(\alpha\sigma_p)]$  versus  $\ln$  strain rate and  $\ln [\sinh(\alpha\sigma_p)]$  vs  $1000/T$  (Fig. 5(b) & (c)) respectively [10]. It is noticed that, deformation mechanism parameters ( $n$  and  $Q$ ) obtained in this study were greater than the generally observed values in the non-ODS steels, which may be attributed to the threshold stress generated due to dislocation/particle interaction [11]. The intercept obtained from the plot between  $\ln [\sinh(\alpha\sigma_p)]$  versus  $\ln$  strain rate gives value of the constant  $A$  ( $1.31 \times 10^{27}$ ).

Sellars–Tegart hyperbolic sine equation was employed to determine the peak flow stress at a constant temperature and strain rate. The rearranged form of the equation is shown below.

$$\sigma_p = \frac{1}{\alpha} \sinh^{-1} \left( \frac{\dot{\epsilon} \exp(Q/RT)}{A} \right)^{1/n} \quad (3)$$

The obtained deformation parameters ( $n$  and  $Q$ ) and material constants ( $\alpha$  and  $A$ ) were substituted in equation 3. The constitutive equation obtained for the ODS-18Cr steel is expressed as

$$\sigma_p = \frac{1}{0.00496} \sinh^{-1} \left( \frac{\dot{\epsilon} \exp(733934/RT)}{1.31 \times 10^{27}} \right)^{1/12.53} \quad (4)$$

The validation of constitutive equation was checked by using Zener-Holloman parameter. The plot between  $\ln(Z)$  versus peak flow stress is shown in Fig. 5(d). The flow stress increases with an increase in Zener parameter. The correlation factor ( $R^2 = 0.98$ ) obtained from the linear fitting of the experimental data indicates that equation 4 well describes the hot deformation behavior of the present steel studied.

#### 4. Conclusions

1. The peak flow stress increases with increasing the strain rate and decreasing the temperature.
2. The strain rate sensitivity ( $m$ ) value increases with increasing temperature but it may not be sufficient for efficient hot working processes.
3. The higher values of deformation parameters ( $n=12.53$  and  $Q = 734$  kJ/mol) obtained in this study indicate the origin of threshold stress due to dislocation/particle interaction.

#### 5. References

- [1] S. Ukai and M. Fujiwara, Perspective of ODS alloys application in nuclear environments, *J. Nucl. Mater.*, 307 (2002) 749-57.
- [2] G. Sundararajan, R. Vijay and A. V. Reddy, Development of 9Cr ferritic-martensitic and 18Cr ferritic oxide dispersion strengthened steels, *Current Sci.*, 105 (2013) 1100-06.
- [3] S. Ohtsuka, S. Ukai, M. Fujiwara, T. Kaito and T. Narita, Improvement of 9Cr-ODS martensitic steel properties by controlling excess oxygen and titanium contents, *J. Nucl. Mater.*, 329 (2004) 372-76.
- [4] M. Ratti, D. Leuvre, M.H. Mathon and Y. de Carlan, Influence of titanium on nano-cluster (Y, Ti, O) stability in ODS ferritic materials, *J.Nucl.Mater.*, 386–388 (2009) 540-43.
- [5] Y. de Carlan, J. L. Bechade, P. Dubuisson, J. L. Seran, P. Billot, A. Bougault, T. Cozzika, S. Doriot, D. Hamon, J. Henry, M. Ratti, N. Lochet, D. Nunes, P. Olier, T. Leblond and M.H. Mathon, CEA developments of new ferritic ODS alloys for nuclear applications, *J. Nucl. Mater.*, 386 (2009) 430-32.
- [6] C.M. Sellars and W.J. McTegart, On the mechanism of hot deformation, *Acta. Metall.*, 14 (1966) 1136-38.
- [7] D. Samantaray, S. Mandal and A.K. Bhaduri, A comparative study on Johnson Cook, modified Zerilli–Armstrong and Arrhenius-type constitutive models to predict elevated temperature flow behaviour in modified 9Cr–1Mo steel, *Comput. Mater. Sci.*, 47 (2009) 568-576.
- [8] Guangming Zhang, Zhangjian Zhou, Hongying Sun, Lei Zou, Man Wang and Shaofu Li, Hot deformation behavior and processing map of a 9Cr ferritic/martensitic ODS steel, *J. Nucl. Mater.*, 455 (2014) 139-44.
- [9] Hongbin Zhang, Kaifeng Zhang, Haiping Zhou, Zhen Lu, Changhong Zhao and Xiaoli Yang, Effect of strain rate on microstructure evolution of a nickel-based superalloy during hot deformation, *Mater. Des.*, 80 (2015) 51-62.
- [10] S. S. Satheesh Kumar, T. Raghu, Pinaki, P. Bhattacharjee, G. Appa Rao and Utpal Borah, Constitutive modeling for predicting peak stress characteristics during hot deformation of hot isostatically processed nickel-base superalloy, *J. Mater. Sci.*, 50 (2015) 6444-56.
- [11] C.M. Sellars and R. A. Petkovic-Luton, Creep of dispersion-strengthened alloys, *Mater. Sci. Eng.*, 46 (1980) 75-87.